Carcinogenesis, 2015, Vol. 36, No. 11, 1407–1418

doi:10.1093/carcin/bgv122
Advance Access publication September 8, 2015
Original Manuscript

ORIGINAL MANUSCRIPT

Dysregulation of Parkin-mediated mitophagy in thyroid Hürthle cell tumors

Junguee Lee, Sujin Ham[1], Min Hee Lee[2], Soung Jung Kim[2], Ji Hoon Park[3], Seong Eun Lee[2], Joon Young Chang[2], Kyong Hye Joung[2], Tae Yong Kim[4], Jin Man Kim[5], Hae Joung Sul, Gi Ryang Kweon[3], Young Suk Jo[2], Koon Soon Kim[2], Young Kee Shong[4], Giuseppe Gasparre[6], Jong Kyeong Chung[1], Anna Maria Porcelli[7,8] and Minho Shong[2,*]

Department of Pathology, Daejeon St. Mary's Hospital, College of Medicine, The Catholic University of Korea, 64 Daeheung-ro, Jung-gu, Daejeon 301-723, Republic of Korea, [1]National Creative Research Initiatives Center for Energy Homeostasis Regulation, Seoul National University, Seoul 151-742, Republic of Korea, [2]Division of Endocrinology, Department of Internal Medicine, Research Center for Endocrine and Metabolic Diseases, Chungnam National University School of Medicine, 282 Munhwa-ro, Jung-gu, Daejeon 301-721, Republic of Korea, [3]Department of Biochemistry, Chungnam National University School of Medicine, 266 Munhwa-ro, Jung-gu, Daejeon 301-747, Republic of Korea, [4]Department of Internal Medicine, University of Ulsan College of Medicine, Asan Medical Center, 388-1 Poongnap-2dong, Songpagu, Seoul 138-736, Republic of Korea, [5]Department of Pathology, Chungnam National University School of Medicine, 266 Munhwa-ro, Jung-gu, Daejeon 301-747, Republic of Korea, [6]Dip. Scienze Mediche e Chirurgiche-DIMEC U.O. Genetica Medica-Pad.11 Pol.S.Orsola-Malpighi, via Massarenti 9 40138, Bologna, Italy, [7]Department of Pharmacy and Biotechnology-FABIT, University of Bologna, Via Irnerio 42, Bologna, Italy and [8]Interdepartmental Industrial Research Center on Health Sciences & Technologies, University of Bologna, Bologna, Italy

*To whom correspondence should be addressed. Research Center for Endocrine and Metabolic Diseases, Chungnam National University Hospital, 640 Daesadong, Jung-gu, Daejeon 301-721, Republic of Korea. Tel: +82 42 280 7161; Fax: +82 42 280 7995; Email: minhos@cnu.ac.kr

Abstract

Abnormal accumulation of defective mitochondria is the hallmark of oncocytes, which are frequently observed in thyroid Hürthle cell lesions. Autophagy is an essential cellular catabolic mechanism for the degradation of dysfunctional organelles and has been implicated in several human diseases. It is yet unknown how autophagic turnover of defective mitochondria in Hürthle cell tumors is regulated. We characterized the expression patterns of molecular markers including Beclin1, LC3, PINK1 and Parkin, which are required for autophagy or mitophagy, in human oncocytic lesions of the thyroid. To undertake mechanistic studies, we investigated autophagy and mitophagy using XTC.UC1 cells, the only *in vitro* model of Hürthle cell tumors. Beclin1 and LC3 were highly expressed in oncocytes of Hürthle cell tumors. XTC.UC1 showed autophagic responses to starvation and rapamycin treatment, whereas they displayed ineffective activation of mitophagy, which is triggered by the coordinated action of PINK1 and Parkin in response to CCCP. This resulted in a decreased turnover of abnormal mitochondria. The mechanisms underlying defective mitophagy and mitochondrial turnover were investigated by genetic analysis of the *PARK2* gene in XTC.UC1 and Hürthle cell tumor tissues. XTC.UC1 and several tumors harbored the V380L mutation, resulting in dysfunctional autoubiquitination and decreased E3 ligase activity. Consistently, oncocytes in Hürthle cell tumors displayed comparable expression of PINK1 but decreased Parkin expression in comparison to normal thyrocytes. The introduction of wild-type Parkin sensitized XTC.UC1 to death induced by CCCP. This study provides a possible etiological basis for oncocytic formation in heterogeneous Hürthle cell tumors through insufficient mitophagy leading to ineffective turnover of aberrant mitochondria caused by dysfunctional Parkin-mediated pathways of mitochondria quality control.

Received: February 23, 2015; **Revised:** August 3, 2015; **Accepted:** August 13, 2015

Abbreviations

FA	follicular adenoma
FC	follicular carcinoma
HA	Hürthle cell adenoma
HC	Hürthle cell carcinoma
IHC	immunohistochemistry
NH	nodular hyperplasia
NHoc	NH with oncocytic change
OCR	oxygen consumption rate
PBS	phosphate-buffered saline
PUB	Parkin UblD-ubiquitin binding
PTCov	oncocytic variant of papillary carcinoma
TOM	translocase of outer mitochondrial membrane

Introduction

Oncocytes (Hürthle cells or Askanazy cells) occurrence and oncocytic change in follicular cells are common events in the thyroid gland. Although oncocytic lesions can be observed in non-neoplastic conditions such as Hashimoto's thyroiditis and nodular hyperplasia (NH), however, they are more prominent and associated with a plethora of pathologic phenotypes in thyroid tumorigenesis, including entities such as oncocytic variant of papillary carcinoma (PTCov), follicular adenoma (FA), follicular carcinoma (FC), Hürthle cell adenoma (HA) and Hürthle cell carcinoma (HC) (1,2). Regardless of the underlying thyroid disease, oncocytes show characteristic cytopathological features, such as an abundant oxyphilic, granular cytoplasm and a large hyperchromatic nucleus. These cytopathologic alterations are caused by excessive accumulation of mitochondria, which usually have morphologic, functional or genetic abnormalities (2). Oncocytes found in HA and HC frequently harbor mutations in mitochondrial DNA that may result in impaired oxidative phosphorylation (2–7). However, oncocytes associated with NH and non-Hürthle cell tumors (e.g. PTCov, FA and FC), have been suggested to develop following a mitochondrial dysfunction secondary to oxidative stress and environmental damage (8). How dysfunctional mitochondria are handled in oncocytes as well as the cellular responses to the accumulation of aberrant mitochondria remain to be investigated.

In recent years, several mitochondria quality control pathways have been identified, which act in a coordinated manner (9). Autophagy, including mitophagy, is regarded to as a critical mitochondria quality control pathway whose activation is linked to impaired mitochondrial bioenergetics (9). Mitophagy may act as a late-stage quality control mechanism by specifically disposing of damaged organelles, and is believed to be an important defense line against disease (10). Recently, extensive investigations demonstrated that initiation of mammalian mitophagy is mediated by the PTEN-induced putative kinase 1 (PINK1) and the E3 ubiquitin ligase Parkin in specific conditions (11,12). Nevertheless, the mechanisms that initiate mitophagy are not completely understood, but they involve multiple steps, including the formation of phagophores and autophagosomes and their subsequent fusion with lysosomes to degrade engulfed organelles, which represents the autophagy process. Autophagy begins with the formation of the hVps34-Beclin1 complex, which is required for nucleation and assembly of the initial phagophore membrane (13–15). Then, autophagy-related (Atg) proteins participate in the subsequent stages of the autophagic process (13–15). The ubiquitin-like conjugation system, Atg8/LC3-phosphatidylethanolamine (PE), contributes to the elongation of phagophore membranes and the maturation of autophagosomes (13–15). Atg8/LC3 lipidation involves Atg4, a cysteine protease that processes pro-LC3 to generate LC3-I (15). LC3-I is activated by Atg7, an E1-like enzyme, and transferred to Atg3, an E2-like enzyme. Concomitantly, LC3-Atg3 is conjugated to PE to form LC3-PE (LC3-II), which is recruited to autophagosomal membranes.

We speculate that excessive accumulation of abnormal mitochondria, the hallmark of oncocytes, results from an imbalance between mitochondrial biogenesis and mitophagy-mediated turnover of abnormal mitochondria. The roles of mitophagy and of cellular pathways that are activated in mitophagy have not been investigated in the context of pathogenesis and tumor behavior in Hürthle cell neoplasms. In this study, we showed that oncocytes in HA and HC showed consistently high levels of Beclin1 and LC3 expression. However, the HC cell line XTC.UC1 showed ineffective activation of mitophagy by CCCP, resulting in decreased turnover of abnormal mitochondria. XTC.UC1 and some Hürthle cell tumors harbored the Parkin mutation V380L, which caused dysfunctional autoubiquitination and decreased E3 ligase activity. Consistently, oncocytes in Hürthle cell tumors displayed comparable expression of PINK1 but decreased Parkin expression in comparison to normal thyrocytes. The introduction of wild-type Parkin sensitized XTC.UC1 to death induced by CCCP. This study provides a possible etiological basis for oncocytic transformation in heterogeneous Hürthle cell tumors through insufficient mitophagy leading to ineffective turnover of aberrant mitochondria caused by dysfunctional Parkin-mediated pathways of mitochondria quality control.

Materials and methods

Subjects and clinical data

In total, 60 patients (11 males and 49 females) were retrospectively enrolled, who underwent thyroidectomy between January 2002 and December 2005 at the Center for Endocrine Surgery, Chungnam National University Hospital; St. Mary's Hospital, Daejeon; or Asan Medical Center, Seoul, South Korea. The 60 cases comprised 6 NHoc, 4 PTCov, one FA, 19 FC, 16 HA and 14 HC. Slides stained with Haematoxylin and Eosin (H&E) were reviewed independently by two pathologists, and a histological diagnosis was made according to the WHO classification of tumors of the endocrine organs (16).

Cell lines, culture conditions and chemicals

The HC cell line XTC.UC1, the human PTC cell line TPC-1 (a kind gift from Dr Masahide Takahashi, Nagoya University, Nagoya, Japan) and the human embryonic kidney cell line HEK293T (a kind gift from Dr Chung, Seoul National University, Seoul, Korea) were grown in Dulbecco's modified Eagle's medium (Gibco®) supplemented with 5% fetal bovine serum (FBS, Gibco®), 100 U/ml penicillin-streptomycin (Gibco®) and 100 μg/ml streptomycin at 37°C in a humidified atmosphere with 5% CO_2 (5). The normal thyroid follicular cell line Nthy-ori 3-1 (Nthy-ori) was provided by the ECACC (European Collection of Cell Culture) and was maintained in RPMI 1640 (Gibco®) supplemented with 5% fetal bovine serum, 100 U/ml penicillin and 100 μg/ml streptomycin. Forty-eight hours after seeding, 10 μM carbonyl cyanide *m*-chlorophenylhydrazone (CCCP) and 10 nM Bafilomycin A1 (both from Sigma–Aldrich Inc.) were applied to cells for 0, 2, 4, 8, 16, 24 and 32 h.

Immunohistochemical analysis

Paraffin-embedded tissue sections (4 μm thick) were de-waxed in xylene and rehydrated in a graded series of ethanol (100 to 80%). Antigens were retrieved with 0.01 M citrate buffer (pH 6.0) by heating the tissue sections in an autoclave at a controlled final temperature of 121°C for 25 min. The tissue sections were then placed in 3% hydrogen peroxide for 5 min to inactivate endogenous peroxidases and blocked for 10 min with non-immune horse serum (UltraTech HRP Kit, Immunotech). The primary antibodies used for

immunohistochemistry (IHC) were as follows: anti-Beclin1 mouse monoclonal (1:300, Santa Cruz Biotechnology), anti-LC3 rabbit monoclonal (1:300, Cell Signaling Technology), anti-PINK1 (1:100, Novus Biologicals), anti-Parkin (1:100, Santa Cruz Biotechnology) and anti-TOM20 rabbit polyclonal (1:500, Santa Cruz Biotechnology). Appropriately diluted primary antibodies were applied for 60 min at room temperature. The tissue sections were then treated with a biotinylated secondary antibody for 30 min at room temperature, followed by UltraTech HRP streptavidin peroxidase (Immunotech) and aminoethylcarbazole solution for additional 10 min at room temperature. Finally, the tissue sections were counterstained with Mayer's haematoxylin for 10 s. Tissue slides were analyzed using an OLYMPUS BX41 microscope.

The immunoreactivities of Beclin1, LC3 and TOM20 were analyzed in oncocytic lesions of all cases. The staining intensity and the percentage of positive oncocytes were calculated for each specimen to obtain a final semi-quantitative score. First, the area percentage of stained cells was scored as follows: score 0, 0%; score 1, 1–25%; score 2, 26–50%; score 3, 51–75% and score 4, 76–100%. Second, the intensity of immunoexpression was scored as follows: score 0, negative; score 1, weakly positive; score 2, moderately positive and score 3, strongly positive. Third, the IHC semiquantitative score was calculated using the following equation: final score = (intensity score × area score) + (intensity score × area score).

Immunofluorescence

Cells were grown on coverslips in six-well plates and treated with MitoTrackerGreen™ or MitoTrackerRed™ (Molecular Probes Inc.). After incubation for 30 min under the specified growth conditions, cells were washed with 1× phosphate-buffered saline (PBS), fixed with PBS containing 4% paraformaldehyde for 15 min and then permeabilized with PBS containing 0.5% Triton X-100 for 5 min at room temperature. Permeabilized cells were blocked with PBS containing 5% bovine serum albumin for 30 min at room temperature. Thereafter, cells were incubated with primary antibodies overnight at 4°C, washed three times with 1× PBS, and incubated at room temperature for 3 h with secondary antibodies. The primary antibodies were anti-Parkin, clone PRK8 (Sigma–Aldrich Inc.), anti-TOM20 (Santa Cruz Biotechnology), and anti-β-catenin (Santa Cruz Biotechnology). Secondary antibodies (goat anti-mouse, goat anti-rabbit) conjugated to Alexa Fluor dyes were obtained from Invitrogen. The stained slides were observed using an Olympus Fluoview FV1000 microscope equipped with a CCD camera (Olympus Corp. Lake Success, NY).

Oxygen consumption rate

Oxygen consumption rate (OCR) was measured using a Seahorse XF-24 analyzer (Seahorse Bioscience). XTC.UC1 and Nthy-ori were seeded onto a XF-24 plate and then incubated in Dulbecco's modified Eagle's medium and RPMI 1640, respectively, supplemented with 5% fetal bovine serum. The day before OCR measurement, the sensor cartridge was calibrated with calibration buffer (Seahorse Bioscience) at 37°C. Three readings were taken after the addition of mitochondrial inhibitors. The mitochondrial inhibitors used were 2 μM oligomycin, 10 μM CCCP and 1 μM rotenone. OCR was automatically calculated and recorded using the sensor cartridge and Seahorse XF-24 software. The plates were saved and the protein concentration was calculated to confirm that there were an approximately equal number of cells in each well.

Electron microscopy analysis

XTC.UC1 and Nthy-ori were fixed after 2 days of culture by immersion in 0.125 M sodium cacodylate buffer, pH 7.3, containing 1% glutaraldehyde and 1% tannic acid immediately after removal of the culture medium. Cells were post-fixed in 0.1 M sodium cacodylate buffer containing 1% osmium tetroxide for 20 min and dehydrated in graded alcohols. Areas containing cells were cut out, removed from the culture dish, and embedded in 1:1 Epon:propylene oxide. Sections were cut orthogonally to the cell monolayer with a diamond knife to generate cross-sections of cells. Thin sections were observed using a FEI Tecnai™ transmission electron microscope.

Results

Baseline characteristics of the study subjects

The mean age of the enrolled subjects was 47.4 ± 12.1 years (range 20–73 years) and the mean tumor size was 3.0 ± 2.0 cm (range 0.2–9.0 cm). The baseline characteristics of each patient are summarized in Table 1 and Supplementary Table 1, available at *Carcinogenesis* Online. H&E staining showed that oncocytic follicular cells from lesions of various types of thyroid disease had abundant eosinophilia in granular cytoplasm (Figure 1 and Supplementary Figure 1, available at *Carcinogenesis* Online). These oncocytic changes were observed in focal areas of lesions in the thyroid glands of patients with NH with oncocytic change (NHoc), FA, FC and PTCov, whereas patients with HA and HC showed diffuse oncocytic changes throughout the entire tumor.

Differential expression of Beclin1 and LC3 in oncocytic lesions of the thyroid gland

Normal thyroid, NH, and follicular tumors

In IHC analyses of normal follicular cells, the autophagosome markers Beclin1 and LC3 were not detected, whereas translocase of outer mitochondrial membrane (TOM) 20 was detected (Supplementary Figure 1, available at *Carcinogenesis* Online). Unexpectedly, the immunoreactivity of Beclin1 and LC3 was not increased in oncocytic lesions in patients with NHoc (Table 1 and Figure 1), although the staining intensity of TOM20 was stronger in NHoc oncocytic lesions than in normal thyroid follicular cells (Figure 1 and Supplementary Figure 1, available at *Carcinogenesis* Online). These findings suggested that in NHoc, autophagosome formation was not enhanced in oncocytes rather than in the surrounding normal follicular cells. In oncocytes in FA and

Table 1. Patients characteristics and IHC results of Beclin1, LC3 and TOM20

	Gender (*n*)				IHC score		
Diagnosis	Male	Female	Age (years)[a]	Size (cm)[a]	Beclin1[b]	LC3[b]	TOM20[b]
NHoc	0	6	51.2 (42–69)	1.2 (0.6–2.1)	0	0	9.0 ± 3.5 (4–12)
PTCov	1	3	45 (34–50)	1.1 (0.2–2.0)	0	0	9.0 ± 2.0 (8–12)
FA	0	1	35.0	4.00	0	0	9.0
FC	5	14	42.7 (26–68)	3.4 (0.9–9.0)	0.4 ± 1.0 (0–4)	0.1 ± 0.5 (0–2)	9 ± 1.5 (8–12)
Total	6	24	44.4 (26–69)	2.7 (0.2–9.0)	0.4 ± 0.8	0.07 ± 0.4	9.0 ± 2.0
HA	3	13	51.1 (41–70)	3.1 (1.0–7.0)	9.1 ± 2.4 (5–12)	11.0 ± 1.6 (8–12)	11.6 ± 0.6 (10–12)
HC	2	12	50.2 (20–73)	3.7 (1.2–8.5)	8.6 ± 2.5 (5–12)	10.6 ± 2.3 (5–12)	11.9 ± 0.3 (11–12)
Total	5	25	50.1 (20–73)	3.4 (1–8.5)	8.8 ± 2.4	10.8 ± 1.9	11.8 ± 0.5

[a]Data represent the median and range.

[b]Data represents the mean ± SE (range). The IHC semiquantitative scores were as follows: (i) area percentage of cells stained: score 0, 0%; score 1, 1–25%; score 2, 26–50%; score 3, 51–75%; score 4, 76–100%. (ii) Intensity of immunoexpression: score 0, negative; score 1, weakly positive; score 2, moderately positive; score 3, strongly positive. (iii) Final score = (intensity score × area score) + (intensity score× area score).

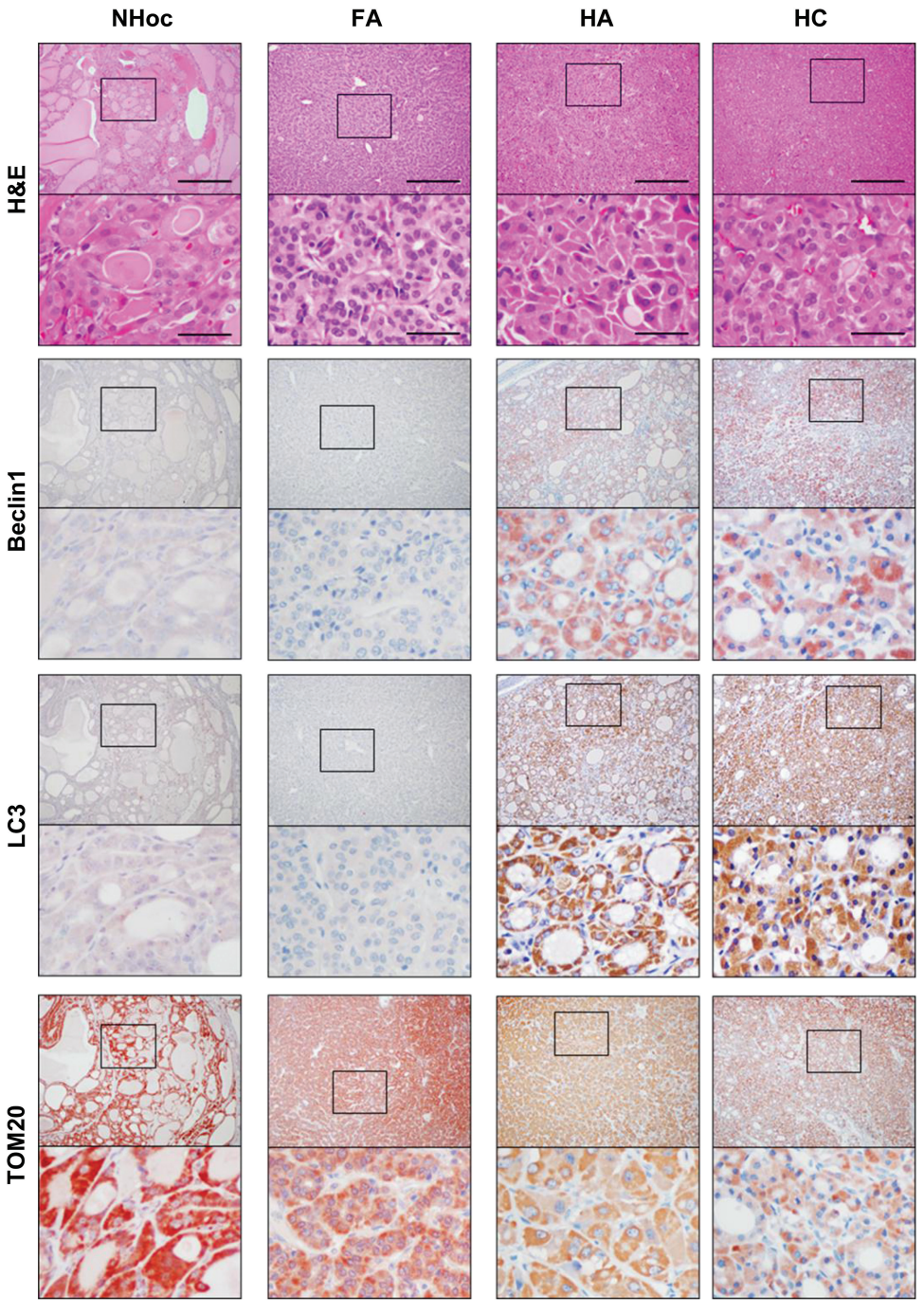

Figure 1. Differential expression of Beclin1 and LC3 in oncocytic lesions of the thyroid gland. Representative images of H&E staining and IHC for Beclin1, LC3, and TOM20 in oncocytes derived from non-neoplastic (NHoc) and neoplastic (FA, HA and HC) thyroid diseases. Scale bar 300 μm. High magnifications of boxed areas in upper images are shown in lower images. Scale bar 25 μm.

FC, the immunoreactivity of Beclin1 and LC3 was extremely weak, whereas that of TOM20 was moderate to strong (Table 1 and Supplementary Table 1, available at *Carcinogenesis* Online; Figure 1 and Supplementary Figure 1, available at *Carcinogenesis* Online).

HA and HC

In contrast to follicular tumors, oncocytes in HA and HC showed uniformly moderate to strong expression of Beclin1 and LC3 (Figure 1). The IHC score (a measure of the expression level) of Beclin1 was 9.1±2.4 (range 5–12) and 8.6±2.5 (range 5–12) in HA and HC, respectively. The IHC score of LC3 was 11.0±1.6 (range 8–12) and 10.6±2.3 (range 5–12) in HA and HC, respectively (Table 1 and Supplementary Table 1, available at *Carcinogenesis* Online). The IHC score of Beclin1 was higher in HA and HC than in FA and FC (Table 1 and Supplementary Table 1, available at *Carcinogenesis* Online). In oncocytes in HA and HC, TOM20 had a strong, homogeneous and fine granular staining pattern (Figure 1).

PTCov

Oncocytes in PTCov showed low expression of Beclin1 and LC3, similar to oncocytes in NHoc. The immunoreactivity of

autophagosome markers was consistently low in all examined PTCov cases that showed extensive oncocytic changes associated with intense expression of TOM20 (Supplementary Figure 1, available at *Carcinogenesis* Online).

Regulation of mitochondrial function in the HC cell line XTC.UC1

In the non-tumor thyroid follicular cell line Nthy-ori, patterns of basal and maximal OCR in response to treatment with mitochondrial complex inhibitors were normal (Figure 2A). In comparison, XTC.UC1 showed a lower basal OCR and a higher basal extracellular acidification rate (ECAR), confirming that mitochondrial respiration was impaired and there was a compensatory increase in glycolysis in culture, as we previously reported (Figure 2A) (5,17).

Confocal microscopic examination of XTC.UC1 labeled with MitoTrackerGreen™ showed larger cytoplasm contained tubular, elongated mitochondrial network compare to Nthy-ori (Figure 2B). Electron microscopy analysis showed that mitochondria of XTC.UC1 were tubular and swollen with poorly developed, sparse cristae in comparison to those of Nthy-ori (Figure 2C), in agreement with their oncocytic origin. We studied the levels of OxPhos complexes subunits in XTC.UC1 cells using western blot analysis. XTC.UC1 cells contained reduced amounts of NADH dehydrogenase subunit 1 (ND1), NDUFB8 subunit of complex I, UQCRC2 subunit of complex III, and COX4 subunit of complex IV (Figure 2D). These findings are consistent with those of a previous report showing that XTC.UC1 cells harbor the homoplasmic m.3571insC mutation in the ND1 subunit of respiratory chain complex I, and therefore lack the whole complex I (17), unlike respiration-competent Nthy-ori cells.

To evaluate the basal or activated autophagy process in XTC.UC1 cells, we measured LC3 processing following serum starvation and rapamycin treatment. LC-II was detected under the basal untreated condition and its level increased with serum starvation, and with 20 nM rapamycin treatment (Figure 2E). In addition, XTC.UC1 retained the autophagy features triggered by starvation and rapamycin-induced inhibition of mTOR kinase, which activate non-selective autophagy (18).

Measurement of autophagy/mitophagy in XTC.UC1

The features of autophagy in XTC.UC1 were further characterized by examining the autophagic flux by western blot analysis of LC3 processing following treatment with Baf A1 and/or CCCP. First, we measured LC3-II formation and the accumulation of p62/sequestosome 1 (p62) in XTC.UC1 treated with Baf A1. After their formation, autophagosomes undergo a stepwise maturation process including fusion events with lysosomes (19,20). Bafilomycin A1 (Baf A1), a vacuolar H(+)-ATPase inhibitor, inhibits the fusion of autophagosomes with lysosomes (21). LC3-II/LC3-I and p62 accumulated in Baf A1-treated Nthy-ori and XTC.UC1, which suggests that fusion between lysosomes

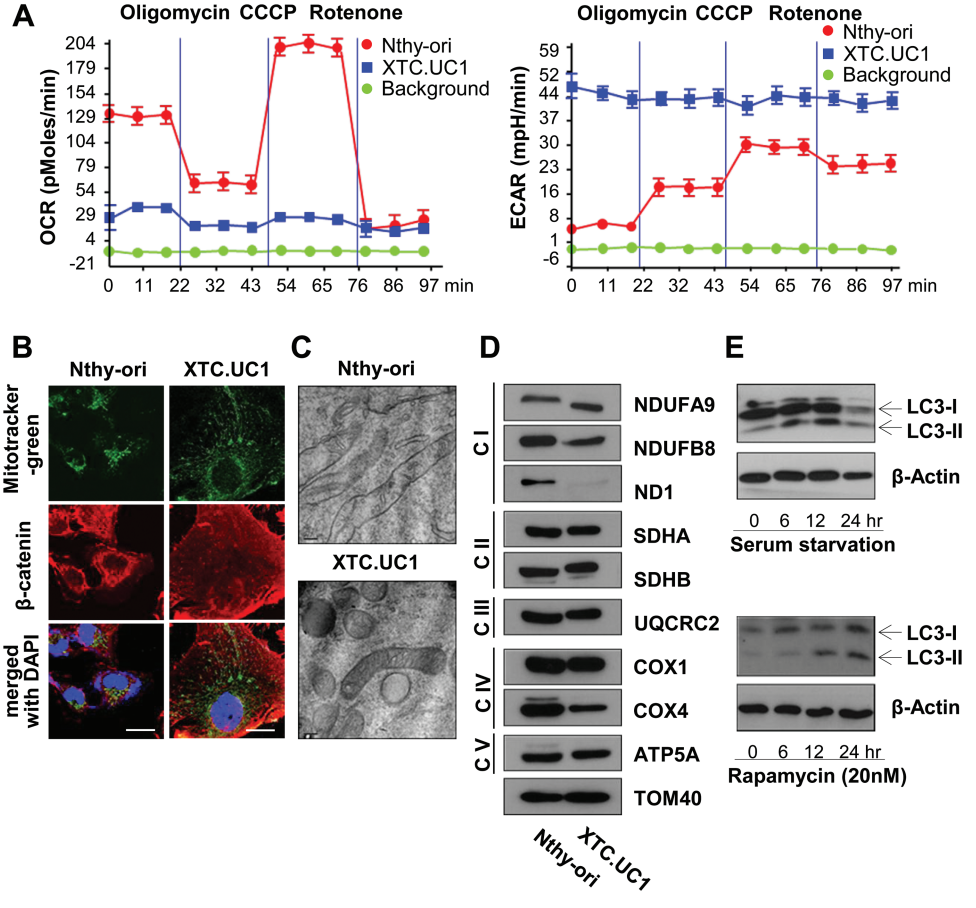

Figure 2. Regulation of mitochondrial function in the HC cell line XTC.UC1. (**A**) XTC.UC1 show a lower basal OCR and a higher basal ECAR than Nthy-ori. (**B**) Confocal microscopy images of XTC.UC1 show an expanded cytoplasm with tubular, elongated mitochondria (labeled green). β-catenin is diffusely localized in the cytoplasm (labeled red). Scale bar 10 μm. (**C**) Electron microscopy images of XTC.UC1 show abnormal, tubular, swollen mitochondria with poorly developed, sparse cristae. (**D**) Western blot analysis of OxPhos subunits demonstrates that XTC.UC1 cells have reduced levels of ND1, NDUFA8 subunit of complex I, and UQCRC2 subunit of complex III. (**E**) Expression of LC3 in XTC.UC1 cells treated with serum starvation, or 20 nM rapamycin was evaluated by western blot analysis.

and autophagosomes was intact in both cell types (Figure 3A). Accumulation of LC3-II and p62 in Baf A1-treated cells suggested that both cell types, Nthy-ori and XTC.UC1, had a low autophagy flux under cell culture conditions. The simultaneous addition of CCCP and Baf A1 robustly promoted LC3-I processing into LC3-II and p62 accumulation in both Nthy-ori and XTC.UC1 (Figure 3B). As mentioned previously, although XTC.UC1 cells do not have competent respiratory capacity due to defective OxPhos complex formation, mitochondrial polarization status is maintained (22) and can be altered by CCCP. CCCP is an uncoupling agent that increases proton permeability across the mitochondrial inner membrane and thus depolarizes mitochondria (10). CCCP has been used extensively in recent years to study mitochondrial damage and to induce the autophagy machinery including that involved in mitophagy (11). Interestingly, ubiquitination of VDAC1, a molecular event in PINK1/Parkin-mediated mitophagy, was reduced in XTC.UC1 treated with CCCP and Baf A1 (Figure 3B). PINK1, a normally short-lived mitochondrial protein kinase, needs to accumulate at high levels on the outer surface of such depolarized mitochondria to trigger Parkin recruitment and mitophagy (23). Parkin ubiquitylates mitochondrial substrates following CCCP-induced uncoupling and mitochondrial

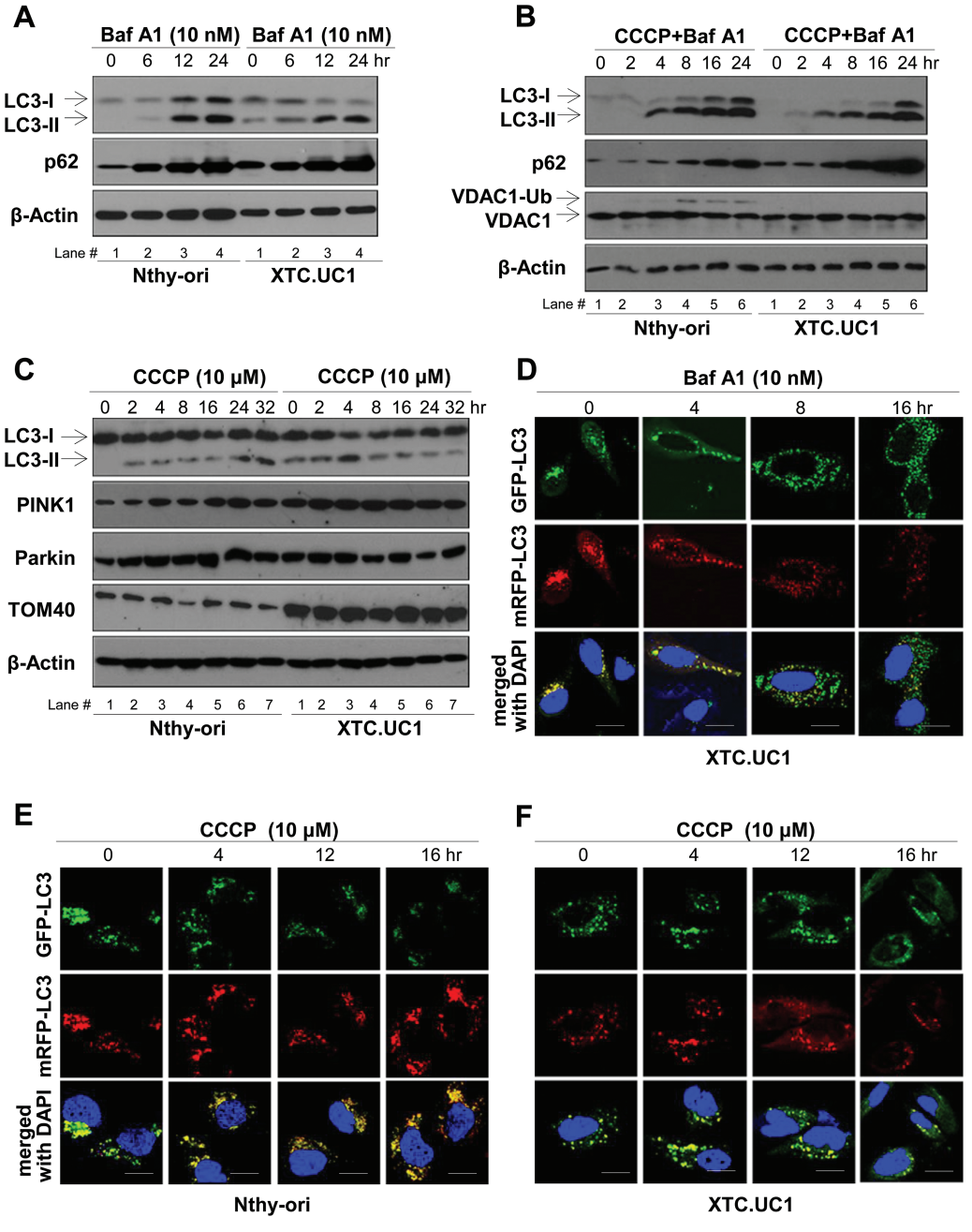

Figure 3. Autophagy/mitophagy flux in XTC.UC1. (**A**, **B**) For flux assays, cells were treated with 10 nM Baf A1 alone (for 6, 12 or 24 h) or 10 μM CCCP plus 10 nM Baf A1 (for 2, 4, 8, 16 or 24 h). Thereafter, cells were harvested at the indicated time points, and levels of LC3-I, LC3-II, p62 and VDAC1 were evaluated by western blot analysis. β-actin was used as a loading control. (**C**) XTC.UC1 and Nthy-ori were treated with 10 μM CCCP alone for 2, 4, 8, 16, 24 or 32 h. Thereafter, levels of LC3-I, LC3-II, PINK1, Parkin and TOM40 were assessed by western blot analysis. β-actin was used as a loading control. (**D**) XTC.UC1 were transfected with GFP-mRFP-LC3 and then treated with 10 nM Baf A1. Yellow puncta (autophagosome) indicate inhibition of autophagy at the lysosomal fusion step in response to Baf A1. (**E**, **F**) Nthy-ori and XTC.UC1 were transfected with GFP-mRFP-LC3 and then treated with 10 μM CCCP. Red puncta (autolysosome) indicate increased autophagic flux in response to CCCP. Scale bar 2.5 μm.

substrates display polyubiquitin chains, which are usually associated with autophagy signaling (10). CCCP treatment gradually increased the protein levels of PINK1 and Parkin for 24 h in Nthy-ori. However, XTC.UC1 had an ~2.5-fold higher level of PINK1 than Nthy-ori under the basal untreated condition and the level of PINK1 did not show further significant increases after 24 h (Figure 3C and Supplementary Figure 2B, available at *Carcinogenesis* Online). Parkin expression in XTC.UC1 was higher than in Nthyh-ori under the basal condition and its level gradually decreased in response to CCCP addition (Figure 3C and Supplementary Figure 2C, available at *Carcinogenesis* Online).

To further examine autophagic flux, XTC.UC1 and Nthy-ori were transfected with tandem GFP-mRFP-LC3 constructs and then fluorescent puncta were observed for 16 h. Cells were either untreated or treated with 10 nM Baf A1 or 10 μM CCCP for 16 h and then fluorescence microscopy was performed. In green/red merged images, there were fewer yellow puncta and more green puncta in Baf A1-treated cells, suggesting that Baf A1 blocks basal autophagic flux in XTC.UC1 (Figure 3D). The uncoupling agent CCCP increased the numbers of yellow and red puncta in Nthy-ori (Figure 3E). However, red puncta formation was not enhanced and green puncta formation was not decreased in XTC.UC1 treated with CCCP (Figure 3F). These observations indicate that CCCP-induced autolysosome formation was hampered in XTC.UC1. The number of green as well as red puncta was decreased at late stages of CCCP treatment in XTC.UC1 (16 h).

Taken together, XTC.UC1 show increased basal autophagic flux, which may be further augmented by CCCP and Baf A1 treatment. These findings indicate that autophagy pathways were constitutively activated in XTC.UC1, which may be a consequence of the presence of abnormal mitochondria with impaired oxidative phosphorylation in these cells. However, XTC.UC1 showed delayed and decreased autophagosome formation and autophagic flux in response to the mitophagy inducer CCCP.

Defective mitophagy pathway in XTC.UC1 cells

Because ubiquitination of VDAC1, which occurs in mitophagy mediated by the PINK1 and Parkin pathways, was specifically impaired, we evaluated the mitophagy flux by measuring lipidated LC3-II levels in mitochondrial fractions of Nthy-ori and XTC.UC1 treated with or without CCCP. LC3-I and LC3-II were detected more strongly in the mitochondrial fraction than in the cytosolic fraction of Nthy-ori with CCCP treatment (Supplementary Figure 3A, available at *Carcinogenesis* Online). While only a small portion of lipidated LC3-II was detected in mitochondrial fraction in CCCP-treated XTC.UC1 (Supplementary Figure 3B, available at *Carcinogenesis* Online). The decreased level of LC3 observed in the mitochondrial fraction of XTC.UC1 in response to CCCP treatment was also supported by the lack of colocalization between GFP-LC3 and MitoTracker fluorescence (Supplementary Figure 3C, available at *Carcinogenesis* Online).

Taken together, these results showed that the HC cell line XTC.UC1 exhibits increased basal autophagosome formation and this can be further increased by treatment with CCCP or Baf A1. However, CCCP-induced autophagosome formation was not sufficient to decrease the level of abnormal mitochondria in the presence of increased LC3-II formation. CCCP-induced autophagy process contains non-selective autophagy and mitophagy, but it has been suggested that non-selective autophagy precedes the mitophagy (24,25).

Our observations of a persistent activation of LC3-II without concomitant decrease of mitochondrial protein such as TOM40 (Figure 3C) suggested that insufficient recruitment of PINK1 and Parkin onto mitochondria may explain the failure of effective turnover of abnormal mitochondria in XTC.UC1. As expected, Nthy-ori treated with CCCP showed clustering of endogenous Parkin into depolarized mitochondria in the perinuclear region (Figure 4A). Mitochondria exist in a dynamic network within living cells, where they undergo fusion and fission events. Mitophagy is preceded by mitochondrial fission, which divides mitochondria into pieces of manageable size for encapsulation into autophagosomes (10). Fission events were evident in CCCP-treated Nthy-ori, indicating the presence of active mitophagy. In XTC.UC1, CCCP treatment did not alter mitochondrial dynamics or the distribution of Parkin at any treatment time (Figure 4B and Supplementary Figure 4, available at *Carcinogenesis* Online). These results suggested that translocation of Parkin into mitochondria is impaired in XTC.UC1 following CCCP-induced mitophagic process (Figure 4B). This perinuclear transport and clustering of mitochondria are Parkin dependent, because this phenomenon was only observed in Parkin-expressing HeLa cells that lack an endogenous Parkin gene (26). The expression of wild-type Parkin in XTC.UC1 restored the translocation of Parkin into mitochondria following CCCP treatment, but the cells continued to show characteristic mitochondrial dynamic networks (Figure 4C). In wild-type Parkin-transfected XTC.UC1 at 12 h CCCP treatment, conglomerates of fragmented mitochondria were visible (Figure 4C). This characteristic change in mitochondria dynamics indicates the later stages of apoptosis showing cleaved caspase-3 (Figure 6A). Collectively, these findings suggest that inadequate and inefficient translocations of Parkin into mitochondria is an important feature of XTC.UC1.

Detection of a mutation in PARK2 in XTC.UC1 cells and Hürthle cell tumors

We examined the expression of PINK1 and Parkin in human thyroid tissues (Figure 5A). Normal thyroid follicular cells expressed low levels of PINK1 and Parkin, whereas oncocytes in PTCov showed moderate to strong immunostaining of PINK1 and Parkin. Interestingly, oncocytes in Hürthle cell tumors showed moderate or low PINK1 staining/expression, and low to extremely weak expression of Parkin (Figure 5A).

Based on the finding that endogenous Parkin has defect in mitophagic process in XTC.UC1, we performed direct sequencing of whole exons of endogenous *PARK2* genomic DNA isolated from these cells. We detected a homozygous point mutation that resulted in the substitution of valine with leucine (V380L) at amino acid residue 380 in the Parkin ubiquitin-binding domain (UblD)-ubiquitin binding (PUB) site (Figure 5B). Parkin is a 465-residue protein that contains two Really Interesting New Gene (RING) motifs linked by a cysteine-rich in-between-RING motif, a newly identified zinc co-ordinating motif termed RING0, and an N-terminal ubiquitin-like domain (Ubl) (Figure 5C). Parkin binds several E2 enzymes, including UbcH7 and UbcH8, as well as the UbcH13/Uev1a E2 heterodimer, which is thought to be responsible for the catalysis of K63-linked ubiquitin chains (27). The N-terminal UblD binds to a C-terminal PUB site to block the interaction with ubiquitin, restricting E2 ubiquitin thioester discharge and Parkin autoubiquitination. This autoinhibition is lost in pathogenic Parkin protein products with UblD mutations (28).

To investigate the structural abnormalities of the gene encoding Parkin (*PARK2*) in patients with HA (n = 5) and HC (n = 2), genomic DNA isolated from the tumor and peritumoral region of HA and HC patients was subjected to direct sequencing. Of seven patients, one HA patient showed identical homozygous G1239C point mutations in exon 10 of *PARK2* that resulted in the V380L substitution found in XTC.UC1. In this patient, this

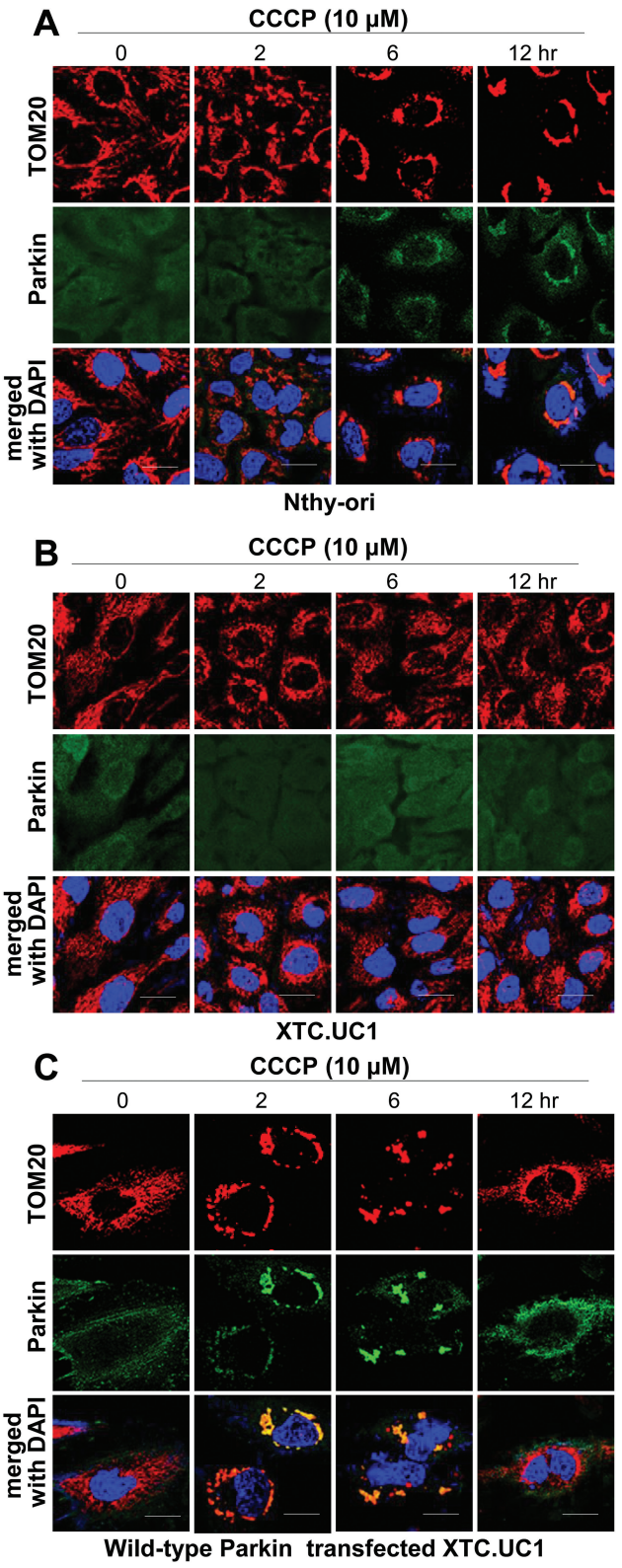

Figure 4. Defective mitophagy pathway in XTC.UC1. (**A**, **B**) Immunofluorescence confocal microscopy analysis of endogenous Parkin in cells treated with CCCP. Scale bar 10 μm. (**C**) In XTC.UC1 cells transfected with wild-type Parkin and treated with CCCP, Parkin translocated into mitochondria. Scale bar 10 μm.

G1239C mutation was not found in the surrounding healthy thyroid tissue (Figure 5D). Strong immunoreactivity against PINK1 was observed in tumor cells of this patient. However, the expression patterns of Parkin (Figure 5E) were similar to those of the patients described in Figure 5A.

As we described earlier, the V380L mutation is located in the PUB site of Parkin that interacts with the N-terminal Ubl domain to form a structure that enhances substrate ubiquitination. Therefore, the V380L mutation would impair ubiquitination and clearance of Parkin substrates by inhibiting the ubiquitin ligase activity of Parkin (29–31). To evaluate whether the V380L mutation affects the autoubiquitination activity of Parkin, an autoubiquitination assay was performed in HeLa transfected with Parkin mutant V380L (Figure 5F). HeLa transfected with the Parkin V380L mutant showed lower levels of Parkin autoubiquitination than HeLa transfected with wild-type Parkin.

A recent study suggests that the E3 ligase activity of Parkin is related to mitochondrial translocation of Parkin (32). Therefore, decreased E3 ligase activity of Parkin V380L mutant in XTC.UC1 may also associated with defective mitochondrial translocation of Parkin. Taken together, the homozygous mutation V380L in the PUB site of Parkin in Hürthle cell tumors and in the HC cell line XTC.UC1 resulted in impaired ubiquitin ligase activity that may have been caused by the dysfunctional intramolecular interaction of mutant Parkin (33,34). These observations suggest that Parkin-mediated mitophagy is altered in Hürthle cell tumors and mutation of the Parkin gene, such as the V380L, may foster the development of oncocytic changes in these tumors.

Expression of wild-type Parkin enhances the death of XTC.UC1 cells

The HC cell line XTC.UC1 exhibited a low level of mitochondrial translocation of Parkin in response to the mitophagy inducer CCCP. In addition, XTC.UC1 harbor Parkin mutant V380L, which may have defects in substrate ubiquitination (33). Therefore, we observed the effects of expressing wild-type Parkin in XTC.UC1. In comparison to XTC.UC1 transfected with a mock vector, XTC.UC1 transfected with a wild-type Parkin cDNA expression plasmid displayed a higher level of PINK1 and more pronounced progressive decreases in p62 and TOM40 levels in the basal state and after CCCP treatment (Figure 6A and Supplementary Figure 5A, available at *Carcinogenesis* Online).

Generally, autophagy and apoptosis are under the control of multiple, common upstream signals (35). Autophagy and apoptosis can occur in the same cell, with autophagy normally preceding apoptosis. In Figure 6, we showed the activation of autophagic and apoptotic processes occurred at 12 and 24 h after CCCP treatment in XTC.UC1 cells transfected with wild-type Parkin. Remarkably, XTC.UC1 transfected with wild-type Parkin showed an increased level of cleaved caspase-3 with CCCP treatment (Figure 6A). XTC.UC1 transfected with wild-type Parkin also showed ubiquitination of VDAC1 (Figure 6A). Early apoptosis (Annexin-V positive/PI negative) and late apoptosis (Annexin-V positive/PI positive) were induced after wild-type Parkin transfection in XTC.UC1 with CCCP treatment (Figure 6B, Supplementary Figure 5B, available at *Carcinogenesis* Online). Although this observation failed to determine whether autophagy precedes apoptosis, the re-expression of wild-type Parkin in XTC.UC1 cells clearly provided the condition for the increase in both autophagy and apoptosis in response to CCCP treatment.

We next attempted to investigate the effect of autophagy induction in XTC.UC1 cells by treating them with rapamycin, a mTOR kinase inhibitor that is widely used for autophagy induction. First, we examined XTC.UC1 viability following 20 nM

rapamycin treatment. The MTT assays revealed that rapamycin treatment reduced XTC.UC1 viability after 12 h (Figure 6C). As we expected, rapamycin treatment of XTC.UC1 cells resulted in a profound decrease in the levels of phosphorylated mTOR and S6 kinases. indicating marked inhibition of mTOR and ribosome S6 kinases (Supplementary Figure 5C, available at *Carcinogenesis* Online). Both activated autophagy and concurrent inhibition of mTOR and S6 kinases, which also possibly regulate the ubiquitin proteasome system, contributed to the death of XTC.UC1 cells (36).

Expression of LC3 did not affect the death rate of XTC.UC1 cells in the absence or presence of CCCP (Figure 6D). LC3 is only a marker of autophagy and cannot initiate autophagy; therefore, it does not affect the cell death response in XTC.UC1 cell treated with CCCP.

Taken together, enhanced mitophagy with acute expression of wild-type Parkin gene promotes apoptotic cell death in Hürthle cells that have intrinsic defects in Parkin-mediated mitophagy.

Discussion

Oncocytes (Hürthle cells or Askanazy cells) are recognized as a subset of cells that are characterized by an abundant cytoplasm in which functionally defective mitochondria accumulate aberrantly. These cells are observed in several pathological conditions. However, the precise mechanism underlying the accumulation of defective mitochondria has not been identified, although several studies have found alterations in mtDNA that may perturb oxidative phosphorylation and thereby speculated a compensatory organelle biogenesis (6,37,38). Autophagy is a critical cellular pathway that performs quality control of cellular organelles, including mitochondria, by recycling dysfunctional cellular components through lysosomal machinery (39). It is conceivable that autophagy or mitophagy is critically linked with the development of oncocytes, a prominent feature of Hürthle cell tumors in the human thyroid gland. Our IHC data clearly showed that oncocytes express Beclin1 and LC3 in Hürthle cells found in non-neoplastic and neoplastic thyroid

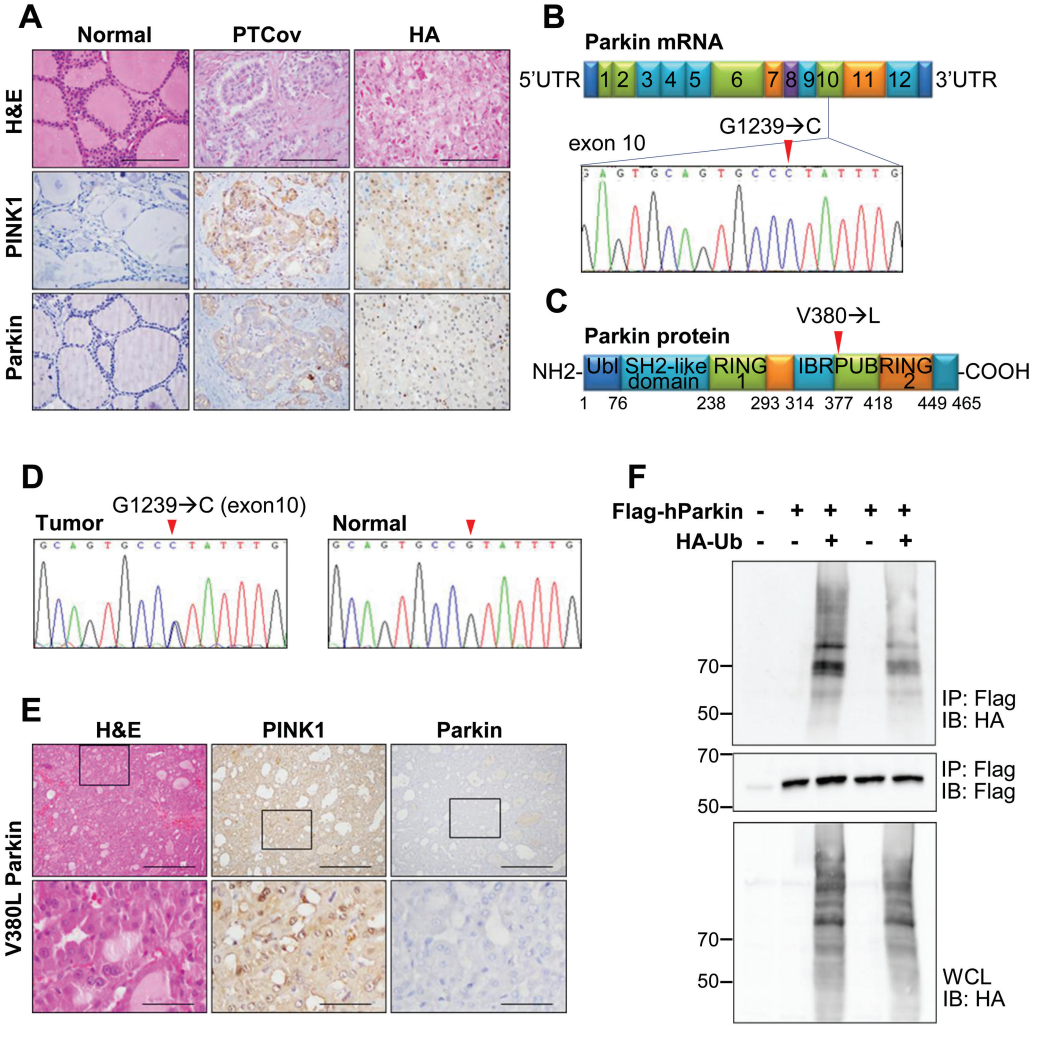

Figure 5. Detection of a mutation in *PARK2* in XTC.UC1 and human Hürthle cell tumors. (**A**) IHC was performed on human thyroid tissues using anti-PINK1 and anti-Parkin antibodies. Scale bar 60 μm. (**B**, **C**) Schematic representation of the *PARK2* gene and the Parkin protein. The point mutation G1239C was detected in exon 10 of *PARK2*. Abbreviations: Ubl, ubiquitin-like domain; R1/2, RING finger domains; IBR, in-between-ring domain; PUB, Parkin UblD-ubiquitin binding. (**D**) Sequencing studies of *PARK2* in human Hürthle cell tumors and the contralateral healthy thyroid. (**E**) H&E staining and IHC labeling for PINK1 and Parkin in a Hürthle cell tumor expressing Parkin mutant V380L. Scale bar 300 μm. High magnifications of boxed areas in upper images are shown in lower images. Scale bar 25 μm. The boxed areas in the ×100 magnifications images are shown in the ×800 magnification images. (**F**) Western blot analysis of Parkin autoubiquitination shows that Parkin mutant V380L is subjected to lower autoubiquitination than wild-type Parkin. Ubiquitin conjugates were detected using hemagglutinin antibodies. HA, hemagglutinin; WCL, whole cell lysate.

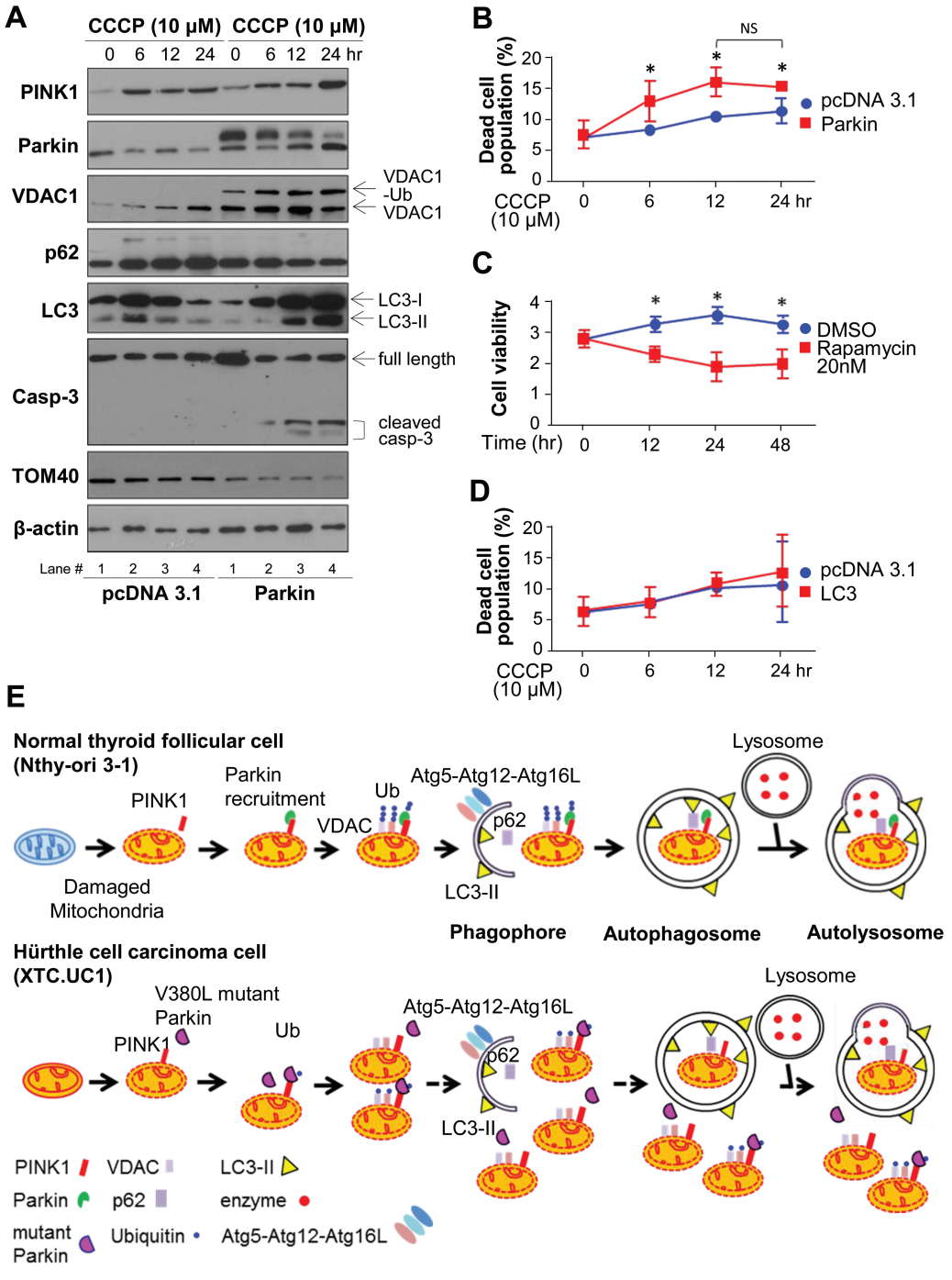

Figure 6. Expression of wild-type Parkin enhances the death of XTC.UC1. (**A**) XTC.UC1 were transfected with a mock vector (pcDNA 3.1) or a wild-type Parkin cDNA expression plasmid, treated with CCCP, and subjected to western blot analysis of PINK1, Parkin, VDAC1, p62, LC3, and caspase-3. TOM40 and β-actin were used as a mitochondrial content and loading control, respectively. (**B**) The percentages of dead cells were calculated among control and wild-type Parkin-transfected XTC.UC1 cultured in the absence or presence of CCCP for up to 24 h. Mean values ± SEM are plotted (* *P*-values are < 0.05). (**C**) Relative cell viability determiend by the MTT cell viability assay was used to assess rapamycin induced cell death. (**D**) The death rates of XTC.UC1 transfected with LC3 cDNA and cultured in the absence or presence of CCCP for up to 24 h were measured using FITC-conjugated Annexin-V and PI. Mean values ± SEM are plotted. (**E**) Schematic model of autophagy/mitophagy regulation in XTC.UC1.

lesions. However, the expression levels of these markers were higher in oncocytes of HA, and HC than in oncocytes of NHoc, PTCov, FA and FC.

Our findings indicate that induction of autophagy and autophagosome formation are common features of oncocytes in HA, and HC that may trigger molecular processes required for the turnover of defective mitochondria in these oncocytic lesions. However, the accumulation of defective mitochondria in oncocytes may be caused by the inability of selective autophagy, namely mitophagy, to sufficiently remove abnormal mitochondria.

However, IHC detection of Beclin1 and LC3 *in vivo* indicated that the level of autophagosome formation was static and thus does not reflect the dynamic turnover of mitochondria.

Autophagic flux assays, such as the LC3 turnover assay, and long-lived protein degradation studies cannot be applied to human thyroid samples (40,41). Therefore, increased expression of Beclin1 and LC3 in Hürthle cell tumors may be inadequate to explain the defective turnover of mitochondria via mitophagy.

To overcome the problems associated with *in vivo* investigations of autophagy, we utilized the HC-derived XTC.UC1 cell line (42), and analyzed mitochondrial status and autophagy. XTC.UC1 lack complex I-mediated mitochondrial respiration, and thus their oxygen consumption was markedly decreased (Figure 2A). In these cells, levels of subunits of OxPhos complexes were markedly decreased, indicating that defects in respiratory complexes underlie the occurrence of defective mitochondria (5,17). As expected, XTC.UC1 showed a high level of LC3-II in basal conditions in the absence of autophagy inducers such as rapamycin and CCCP. Although XTC.UC1 lack mitochondrial respiration, CCCP, which induces mitophagy by inducing mitochondrial depolarization (11), increased conversion of LC3-I into LC3-II.

As shown in Figure 3C and Supplementary Figure 3, available at *Carcinogenesis* Online, CCCP-treated XTC.UC1 showed significant conversion of LC3-I into LC3-II, but the level of LC3-II was only increased in the mitochondrial fraction of Nthy-ori, not in that of XTC.UC1. However, XTC.UC1 did not show effective mitochondrial localization of Parkin in response to CCCP treatment, indicating inefficient mitophagy. Taken together, these results indicate that the autophagy/mitophagy inducer CCCP triggers autophagosome or autolysosome formation, but that mitophagy for effective turnover of abnormal mitochondria is not induced in XTC.UC1. Again, these results may suggest that XTC.UC1 has intact process of non-selective autophagy, but they may have defects in mitophagy regulated by PINK1 and Parkin.

The PINK1-Parkin pathway plays a critical role in the maintenance of mitochondria quality control by triggering mitophagy of abnormal mitochondria (9,43). Low immunoexpression of PINK1 and Parkin was detected in Hürthle cell tumors. Surprisingly, in XTC.UC1, Parkin failed to efficiently translocate into mitochondria, which is a critical molecular step in PINK1-mediated mitophagy following CCCP treatment. Based on these findings, ineffective turnover of abnormal mitochondria in XTC.UC1 may be caused by inefficient mitochondrial translocation of Parkin associated with decreased ligase activity of mutant Parkin in mitochondria (Figure 6E).

To further substantiate the finding that defective ubiquitination of Parkin substrates can cause ineffective turnover of abnormal mitochondria, we revealed a point mutation in the PUB domain of Parkin (V380L) in XTC.UC1. This mutation has been reported in familial Parkinson's disease (44) and may be a genetic cause of mitochondrial dysfunction in Parkinson's disease. Within the PUB domain, there is a binding motif for the Ubl domain that is located in the N-terminal region of Parkin. Binding between the Ubl and PUB domains provides the structural autoinhibition that prevents autoubiquitination of Parkin and may affect its stability (33).

Of seven patients with Hürthle cell tumors, one harbored the tumor-specific Parkin mutant V380L, which suggested that this genetic alteration may be an underlying factor for the excessive accumulation of abnormal mitochondria in Hürthle cell tumors, and perhaps contribute to the accumulation of mtDNA mutations typical of oncocytic tumors (45) The functional role of wild-type Parkin was demonstrated by measuring cell death and turnover of abnormal mitochondria in XTC.UC1. How transfection of wild-type Parkin enhanced the death of XTC.UC1 warrants further investigation. However, acute overexpression of wild-type Parkin enhanced the removal of accumulated abnormal mitochondria that induced increase of apoptosis. Recently, Veeriah *et al.* (46) suggested that *PARK2* acts as a tumor suppressor in certain forms of non-neuronal cell cancer. Several studies indicate that *PARK2* mutations are mostly present in the RING finger and SH2-like domains (46). Although these mutations may not be related to the autoinhibition of Parkin, they abrogate the ability of Parkin to block tumor cell growth and to ubiquitinate cyclins (33). Here, we suggest that the Parkin mutant V380L is a tumor-specific mutation found in Hürthle cell tumors and is associated with abnormal mitophagy.

In summary, oncocytic cells found in Hürthle cell tumors showed ineffective turnover of abnormal mitochondria that may be caused by decreased E3 ligase activity associated with dysfunctional translocation of Parkin into mitochondria. In addition, some patients with Hürthle cell tumors harbored a tumor-specific mutation in Parkin (V380L), and this may explain why oncocytes form in a specific group of heterogeneous Hürthle cell tumors.

Supplementary material

Supplementary materials and methods, Supplementary Figures 1–5 and Supplementary Table 1 can be found at http://carcin.oxfordjournals.org/

Funding

Basic Science Research Program through the National Research Foundation of Korea (NRF) funded by the Ministry of Science, ICT and Future Planning, Korea (2012R1A2A1A03002833, 2014M3A9D8034464). Ministry of Science, ICT and Future Planning, Research fund of Chungnam National University (NRF-2014R1A6A1029617 to M.S.). Italian Association for Cancer Research AIRC IG 14242; EU-Marie Curie Action ITN-People grant MEET – Mitochondrial European Educational Training GA: 317433 (G.G. and A.M.P.). National Creative Research Initiatives grant funded by the Korea government (MSIP) (no. 2010-0018291 to S.H. and J.C.).

Conflict of Interest Statement: None declared.

References

1. Mete, O. et al. (2010) Oncocytes, oxyphils, Hürthle, and Askanazy cells: morphological and molecular features of oncocytic thyroid nodules. Endocr. Pathol., 21, 16–24.
2. Máximo, V. et al. (2012) The biology and the genetics of Hurthle cell tumors of the thyroid. Endocr. Relat. Cancer, 19, R131–R147.
3. Máximo, V. et al. (2000) Hürthle cell tumours of the thyroid. A review with emphasis on mitochondrial abnormalities with clinical relevance. Virchows Arch., 437, 107–115.
4. Gasparre, G. et al. (2007) Disruptive mitochondrial DNA mutations in complex I subunits are markers of oncocytic phenotype in thyroid tumors. Proc. Natl Acad. Sci. USA, 104, 9001–9006.
5. Bonora, E. et al. (2006) Defective oxidative phosphorylation in thyroid oncocytic carcinoma is associated with pathogenic mitochondrial DNA mutations affecting complexes I and III. Cancer Res., 66, 6087–6096.
6. Máximo, V. et al. (2002) Mitochondrial DNA somatic mutations (point mutations and large deletions) and mitochondrial DNA variants in human thyroid pathology: a study with emphasis on Hürthle cell tumors. Am. J. Pathol., 160, 1857–1865.
7. Fusco, A. et al. (2005) Point mutation in GRIM-19: a new genetic lesion in Hurthle cell thyroid carcinomas. Br. J. Cancer, 92, 1817–1818.
8. Katoh, R. et al. (1998) Solitary, multiple, and familial oxyphil tumours of the thyroid gland. J. Pathol., 186, 292–299.
9. Ashrafi, G. et al. (2013) The pathways of mitophagy for quality control and clearance of mitochondria. Cell Death Differ., 20, 31–42.

10. Youle, R.J. et al. (2011) Mechanisms of mitophagy. Nat. Rev. Mol. Cell Biol., 12, 9–14.
11. Narendra, D. et al. (2008) Parkin is recruited selectively to impaired mitochondria and promotes their autophagy. J. Cell Biol., 183, 795–803.
12. McBride, H.M. (2008) Parkin mitochondria in the autophagosome. J. Cell Biol., 183, 757–759.
13. He, C. et al. (2009) Regulation mechanisms and signaling pathways of autophagy. Annu. Rev. Genet., 43, 67–93.
14. Tanida, I. (2011) Autophagosome formation and molecular mechanism of autophagy. Antioxid. Redox Signal., 14, 2201–2214.
15. Wang, W. et al. (2013) The carboxyl-terminal amino acids render pro-human LC3B migration similar to lipidated LC3B in SDS-PAGE. PLoS One, 8, e74222.
16. Volante, M. et al. (2010) Poorly differentiated thyroid carcinoma: 5 years after the 2004 WHO classification of endocrine tumours. Endocr. Pathol., 21, 1–6.
17. Porcelli, A.M. et al. (2010) The genetic and metabolic signature of oncocytic transformation implicates HIF1alpha destabilization. Hum. Mol. Genet., 19, 1019–1032.
18. Li, L. et al. (2013) Starvation-induced autophagy is regulated by mitochondrial reactive oxygen species leading to AMPK activation. Cell. Signal., 25, 50–65.
19. Bjørkøy, G. et al. (2005) p62/SQSTM1 forms protein aggregates degraded by autophagy and has a protective effect on huntingtin-induced cell death. J. Cell Biol., 171, 603–614.
20. Geisler, S. et al. (2010) PINK1/Parkin-mediated mitophagy is dependent on VDAC1 and p62/SQSTM1. Nat. Cell Biol., 12, 119–131.
21. Eskelinen, E.L. (2005) Maturation of autophagic vacuoles in mammalian cells. Autophagy, 1, 1–10.
22. Porcelli, A.M. et al. (2009) Respiratory complex I dysfunction due to mitochondrial DNA mutations shifts the voltage threshold for opening of the permeability transition pore toward resting levels. J. Biol. Chem., 284, 2045–2052.
23. Eiyama, A. et al. (2015) PINK1/Parkin-mediated mitophagy in mammalian cells. Curr. Opin. Cell Biol., 33, 95–101.
24. Yoshii, S.R. et al. (2011) Parkin mediates proteasome-dependent protein degradation and rupture of the outer mitochondrial membrane. J. Biol. Chem., 286, 19630–19640.
25. Hayashi-Nishino, M. et al. (2009) A subdomain of the endoplasmic reticulum forms a cradle for autophagosome formation. Nat. Cell Biol., 11, 1433–1437.
26. Denison, S.R. et al. (2003) Alterations in the common fragile site gene Parkin in ovarian and other cancers. Oncogene, 22, 8370–8378.
27. Olzmann, J.A. et al. (2007) Parkin-mediated K63-linked polyubiquitination targets misfolded DJ-1 to aggresomes via binding to HDAC6. J. Cell Biol., 178, 1025–1038.
28. Burchell, L. et al. (2012) Small, N-terminal tags activate Parkin E3 ubiquitin ligase activity by disrupting its autoinhibited conformation. PLoS One, 7, e34748.
29. Winklhofer, K.F. (2014) Parkin and mitochondrial quality control: toward assembling the puzzle. Trends Cell Biol., 24, 332–341.
30. Wauer, T. et al. (2013) Structure of the human Parkin ligase domain in an autoinhibited state. EMBO J., 32, 2099–2112.
31. Yao, D. et al. (2004) Nitrosative stress linked to sporadic Parkinson's disease: S-nitrosylation of parkin regulates its E3 ubiquitin ligase activity. Proc. Natl Acad. Sci. USA., 101, 10810–10814.
32. Zheng, X. et al. (2013) Parkin mitochondrial translocation is achieved through a novel catalytic activity coupled mechanism. Cell Res., 23, 886–897.
33. Liu, F. et al. (2011) Policing Parkin with a UblD. EMBO J., 30, 2757–2758.
34. Beasley, S.A. et al. (2007) Structure of the Parkin in-between-ring domain provides insights for E3-ligase dysfunction in autosomal recessive Parkinson's disease. Proc. Natl. Acad. Sci. USA, 104, 3095–3100.
35. Mariño, G. et al. (2014) Self-consumption: the interplay of autophagy and apoptosis. Nat. Rev. Mol. Cell Biol., 15, 81–94.
36. Noack, M. et al. (2015) Activation of autophagy by rapamycin does not protect oligodendrocytes against protein aggregate formation and cell death induced by proteasomal inhibition. J. Mol. Neurosci., 55, 99–108.
37. Máximo, V. et al. (2000) Mitochondrial DNA 'common' deletion in Hürthle cell lesions of the thyroid. J. Pathol., 192, 561–562.
38. Müller-Höcker, J. et al. (1998) Hashimoto thyroiditis is associated with defects of cytochrome-c oxidase in oxyphil Askanazy cells and with the common deletion (4,977) of mitochondrial DNA. Ultrastruct. Pathol., 22, 91–100.
39. Glick, D. et al. (2010) Autophagy: cellular and molecular mechanisms. J. Pathol., 221, 3–12.
40. Mizushima, N. et al. (2007) How to interpret LC3 immunoblotting. Autophagy, 3, 542–545.
41. Mizushima, N. et al. (2010) Methods in mammalian autophagy research. Cell, 140, 313–326.
42. Savagner, F. et al. (2001) Mitochondrial activity in XTC.UC1 cells derived from thyroid oncocytoma. Thyroid, 11, 327–333.
43. Park, J. et al. (2006) Mitochondrial dysfunction in Drosophila PINK1 mutants is complemented by parkin. Nature, 441, 1157–1161.
44. Petruzzella, V. et al. (2012) Dysfunction of mitochondrial respiratory chain complex I in neurological disorders: genetics and pathogenetic mechanisms. Adv. Exp. Med. Biol., 942, 371–384.
45. Gasparre, G. et al. (2013) Relevance of mitochondrial genetics and metabolism in cancer development. Cold Spring Harb. Perspect. Biol., 5.
46. Veeriah, S. et al. (2010) Somatic mutations of the Parkinson's disease-associated gene PARK2 in glioblastoma and other human malignancies. Nat. Genet., 42, 77–82.